A novel induced pluripotent stem cell model of Schwann cell differentiation reveals *NF2*-related gene regulatory networks of the extracellular matrix

Olivia Lazaro[1,*], Sihong Li[1,2,*], William Carter[1], Oluwamayowa Awosika[1], Sylvia Robertson[1], Brooke E. Hickey[3], Steven P. Angus[3,4,5], Austin House[1], Wade D. Clapp[3,4,7], Abdul S. Qadir[1,#], Travis S. Johnson[1,3,4,6,#], Steven D. Rhodes[3,4,7,8#]

[1]Indiana Bioscience Research Institute

[2]Indiana University School of Public Health

[3]Department of Pediatrics, Herman B Wells Center for Pediatric Research, Indiana University School of Medicine, Indianapolis, IN, USA

[4]Melvin and Bren Simon Comprehensive Cancer Center, Indiana University School of Medicine, Indianapolis, IN USA

[5]Department of Pharmacology and Toxicology, Indiana University School of Medicine, Indianapolis, IN, USA

[6]Center for Computational Biology and Bioinformatics

[7]Department of Medical and Molecular Genetics, Indiana University School of Medicine, Indianapolis, IN, USA

[8]Division of Pediatric Hematology/Oncology/Stem Cell Transplant, Indiana University School of Medicine, Indianapolis, IN, USA

[#]Corresponding authors: Abdul S. Syed (asyed@indianabiosciences.org), Travis S. Johnson (johnstrs@iu.edu), Steven D. Rhodes (sdrhodes@iu.edu)

Abstract: Schwann cells are vital to development and maintenance of the peripheral nervous system and their dysfunction has been implicated in a range of neurological and neoplastic disorders, including *NF2*-related schwannomatosis. We developed a novel human induced pluripotent stem cell (hiPSC) model to study Schwann cell differentiation in health and disease. We performed transcriptomic, immunofluorescence, and morphological analysis of hiPSC derived Schwann cell precursors (SPCs) and terminally differentiated Schwann cells (SCs) representing distinct stages of development. To validate our findings, we performed integrated, cross-species analyses across multiple external datasets at bulk and single cell resolution. Our hiPSC model of Schwann cell development shared overlapping gene expression signatures with human amniotic mesenchymal stem cell (hAMSCs) derived SCs and *in vivo* mouse models, but also revealed unique features that may reflect species-specific aspects of Schwann cell biology. Moreover, we identified gene co-expression modules that are dynamically regulated during hiPSC to SC differentiation associated with ear and neural development, cell fate determination, the *NF2* gene, and extracellular matrix (ECM) organization. By cross-referencing results between multiple datasets, we identified new genes potentially associated with *NF2* expression. Our hiPSC model further provides a tractable platform for studying Schwann cell development in the context of human disease.

Keywords: Schwann cells, NF2, Schwannoma, hiPSC, RNA-seq, scRNA-seq, gene co-expression analysis, systems biology, extracellular matrix

41 **Abbreviations:**

hiPSC	Human induced pluripotent stem cells
SC	Schwann cells
SPC	Schwann cell precursors
iSC	Immature SCs
mSC	Myelinating SCs
tSC	Transition SCs
pmSC	Pro-myelinating SCs
nmSC	Not-myelinating SCs
nm(R)SC	Non-myelinating (Remak) SCs

42

43 **INTRODUCTION**

44 Schwann cells are glial cells that originate in the neural crest and play a crucial role in
45 myelinating peripheral nerves[1]. Myelination enhances the speed and efficiency of nerve
46 conduction by forming a single spiraling myelin sheath around an axon [2]. Non-myelinating
47 Schwann cells also provide unmyelinated axons with trophic support and mechanical cushioning
48 [3]. Deregulated Schwann cell development can give rise to tumors of the peripheral and cranial
49 nerves called schwannomas, which can have unpredictable clinical behavior, significant
50 morbidities, and exceedingly limited therapeutic options available for their treatment [4].

51 Vestibular schwannomas are tumors that involve the eight cranial nerves, which are critical for
52 hearing and balance. Affected individuals often suffer significant morbidities including tinnitus,
53 sensorineural hearing loss, and impairment of balance and coordination [5]. Most vestibular
54 schwannomas occur unilaterally; however, approximately 10% of cases involve both sides and
55 are frequently associated with an autosomal dominant, heritable genetic condition called *NF2*-
56 related schwannomatosis (*NF2*-SWN, formally known as neurofibromatosis type 2 [5, 6]. *NF2*-
57 SWN is caused by pathogenic variants in the *NF2* tumor suppressor gene, which encodes
58 Merlin, a cytoskeletal adaptor protein with diverse biochemical functions [7]. The development of
59 bilateral vestibular schwannomas is a hallmark of *NF2*-SWN [8].

60 To better understand the molecular mechanisms underlying schwannoma genesis in *NF2*-SWN,
61 the development of new model systems for normal and diseased Schwann cells is imperative.
62 Human induced pluripotent stem cells (hiPSCs) have demonstrated promise in modeling a
63 multitude of neurological diseases and cell types, including but not limited to hiPSC-derived
64 astrocytes [9-12], microglia [13-15], and neurons [16, 17]. Direct conversion of human
65 fibroblasts to hiPSC-deviled neurons has also been achieved [17]. These iPSC-derived cells
66 have been employed to interrogate neuropsychiatric diseases [18-20], neurodegenerative

67 diseases [13, 20, 21], and gliomas [22-24]. However, beyond gliomas, considerably less
68 progress has been made in the field of iPSC modeling of peripheral nervous system derived
69 tumors including schwannoma [25].

70 To address this unmet need, we have developed a novel hiPSC Schwann cell model that can
71 be used to study Schwann cell differentiation in health and disease. Here, we performed
72 transcriptomic profiling of hiPSCs at multiple stages of Schwann cell differentiation to unveil
73 broad networks of differentially expressed genes (DEGs) associated with Schwann cell lineage
74 maturation and compare them to developmental stages outlined in other studies (**Table 1**). To
75 further characterize complex gene regulatory networks (GRNs) associated with Schwann cell
76 differentiation, we employed a systems biology approach, utilizing weighted gene co-expression
77 network analysis (WGCNA) to identify modules of transcriptionally associated genes [26] and to
78 study their temporal dynamics in unison. We further refine the putative roles of these modules
79 using functional enrichment analysis [27]. To validate our findings, we compared the DEGs and
80 gene modules derived from our hiPSC induced Schwann cells with two independent single cell
81 and bulk transcriptomic datasets of human Schwann cell differentiation [28] and mouse sciatic
82 nerve development [29].

83 **METHODS**

84 **hiPSC generation**

85 hiPSC lines were generated from neonatal human dermal fibroblasts (HDFn) from Invitrogen
86 (Catalog #: C-004-5C) using an Epi5™ Episomal iPSC Reprogramming Kit (ThermoFisher
87 Scientific) according to manufacturer's protocol. Transduced cells were plated on growth factor
88 reduced Matrigel (Corning, 356231) coated culture dishes in the presence of ROCK inhibitor and
89 maintained in Essential 8 (E8) medium. iPSC colonies were mechanically isolated and expanded
90 until at least passage 12 before differentiation. iPSCs were characterized by staining with

91 pluripotency markers and embryoid body (EB) formation. *Mycoplasma* testing was performed
92 prior to Schwann cell differentiation.

93 **Schwann cell differentiation from hiPSCs**

94 The human iPSC line IBRI.101.J was differentiated into Schwann cells using a six-stage
95 protocol over 31 days as described previously [30]. To start differentiation, the IBRi 101.J hiPSC
96 line was seeded on Matrigel-coated culture plate in E8 media. When the cells reached 50-60%
97 confluency, the culture medium was replaced with Schwann cell basal 1 (SCB1) media (NDM
98 containing 1x N2, 1x B27, 0.005% BSA, 2 mM GlutaMAX, 0.11 mM b-mercaptoethanol in
99 advanced DMEM/F12 and Neurobasal medium (1:1 mix)) with 3 μM CHIR and 20 μM
100 SB431542 for 6 days. On day 7, cells were fed with SCB1 media with 3 μM CHIR, 20 μM
101 SB431542 and 50 ng/mL neuregulin 1 (NRG1) through day 24. SCB1 media was replaced with
102 fresh medium daily, and the cells were routinely dissociated and expanded once they reached
103 80% confluence with Accutase treatment. On day 25, media was switched to Schwann cell
104 basal 2 (SCB2) media (DMEM, 1x NEAA, 1x BME and 2% FBS) with 200 ng/mL NRG1, 4
105 ng/mL Forskolin, 100 nM RA-all Trans and 10 ng/mL platelet derive growth factor subunit B
106 (PDGF-BB) for 3 days, then to SCB2 media with 200 ng/mL NRG1 and 10 ng/mL PDGF-BB for
107 2 days, and finally to SCB2 media with 200 ng/mL NRG1 for 2 more days. By day 31, terminal
108 differentiation to Schwann-like cells was completed. Samples were collected at days 0, 3, 6, 12,
109 18, 24 and at a uniform 70% confluency in all cases. Cell pellets were collected, and flash
110 frozen at -80°C from three wells for subsequent RNA extraction and RNA-seq, while one well
111 was retained for continued passaging to the next stage.

112 **Immunoflourescence staining of hiPSC-derived Schwann cell precursors (SCPs) and SCs**

113 We used immunofluorescence (IF) analysis to characterize hiPSC differentiation to SCPs and
114 SCs [31]. For immunostaining, cells were fixed with 4% Paraformaldehyde for 10 minutes. The
115 fixed cells were washed with PBS three times and then blocked and permeabilized with 0.3%
116 Triton X-100 (Sigma) in 1% Bovine Serum Albumin (Life Technologies) and 10% FBS for 1 hour
117 at room temperature. Cells were then incubated with primary antibodies 1:200 dilution of S100β
118 (Abcam #AB52642), 1:50 dilution of p75 (Abcam #AB3125), 1:100 dilution of HOXb7 (Santa
119 Cruz #sc-81292), and 1:500 dilution of GAP43 (Abcam #AB12274) at 4 °C overnight, then with
120 conjugated secondary antibodies at 1:500 dilution for 1 hour at room temperature. The
121 coverslips were mounted on slides with DAPI to stain the nuclei (VectorLabs). Images were
122 captured with an LSM 780 confocal microscope running Zen Black software.
123 Immunocytochemistry analysis confirmed the expression of S100β, p75, HOXb7, and GAP43.

124

125 **RNA extraction, library preparation and sequencing**

126 RNA was extracted using phenol-chloroform extraction with TRIzol LS Reagent (Life
127 Technologies Corporation, #10296028). 1mL of TRIzol LS Reagent was added to flash frozen
128 cell pellets followed by 0.2 mL of chloroform. Tubes were shaken by hand for 15 seconds and
129 incubated at room temperature for 2-3 minutes. Centrifugation was performed on samples at
130 4°C for 15 minutes at 13,200 rpm. The aqueous phase was transferred to an RNase-free tube
131 and an equal amount of 70% ethanol was added to each sample for a final concentration of
132 35%. Samples were vortexed and binding and washing of RNA was carried out according to the
133 instructions of Invitrogen's PureLink™ RNA Micro Scale Kit #12183016. Samples were eluted in
134 20 µL RNase-free water. The quality and quantity of RNA was determined using a NanoDrop™
135 Spectrophotometer (Thermo Scientific).

136 A total of 21 samples, 3 replicates for each of the 7 timepoints, were shipped overnight on dry
137 ice to Novogene for quality control, library preparation and RNA-sequencing as further
138 described below.

139 **Initial processing of RNA-sequencing data**

140 CASAVA (Consensus Assessment of Sequence And Variation) was used for base recognition
141 through the Illumina Genome Analyzer. Raw reads were removed if they contained adapter
142 sequences, greater than 10% undetermined bases, or more than 50% low-quality bases (quality
143 scores less than 5). Sequenced reads were then aligned to the GRCh38 Genome using HISAT2
144 v2.0.5 and quantified with feature counts v1.5.0-p3. FPKM values were calculated from the read
145 counts and CDS lengths for each gene across all timepoints and replicates.

146 **Differential Gene Expression analysis**

147 Differential gene expression analysis was performed with edgeR v3.22.5. The $\log_2$ fold change
148 (Log_2FC) was calculated between groups and the p-values (P) were corrected using the
149 Benjamini & Hochberg method (BH) to account for the false discovery rate (FDR). Each
150 timepoint (day 3, 6, 12, 18, 24, 31) was compared to baseline (day 0), resulting in 6 pairwise
151 comparisons. DEGs with $Log_2FC > 5.0$ and $FDR < 0.001$ were identified for each comparison.
152 Functional enrichment analysis was performed on DEGs from each comparison using
153 clusterProfiler v3.8.1 to test the statistical enrichment for genes within the Reactome, DO
154 (Disease Ontology), and DisGeNET databases. Terms with $FDR < 0.05$ were considered
155 enriched. Functional enrichment on other gene sets derived from this analysis was performed
156 using ToppGene [32].

157 **Network Construction and Module Detection with WGCNA and ImQCM**

158 Statistical analysis was performed using R (v4.1.1.). Genes with the lowest 10% mean FPKM
159 across all timepoints were removed. Ensembl IDs for the filtered genes were converted to
160 HGNC gene symbols using biomaRt (v2.52.0) and the Ensembl gene IDs from the Genome
161 assembly GRCh38.p14. For HGNC symbols with multiple corresponding Ensembl IDs, the
162 Ensembl ID with the highest average FPKM was used. WGCNA module generation was
163 conducted with an unsigned Pearson correlation coefficient (PCC) matrix. Soft thresholding
164 power was calculated to reduce noise for gene correlations and emphasize correlations
165 between genes per WGCNA documentation. A block size of 22000 was used for network
166 construction and module detection as described previously [26]. Eigengenes were subsequently
167 calculated for each module detected by WGCNA. Gene modules whose eigengene values
168 changed significantly ($P<0.05$) for at least one timepoint were identified by ANOVA. Enrichment
169 analysis was performed using clusterProfiler to identify significantly associated ontology terms
170 for each module. All ontologies contained in clusterProfiler were evaluated, including BP
171 (biological process), CC (cellular component), and MF (molecular function).

172 **Evaluating Schwann cell differentiation from amniotic mesenchymal stem cells via single**
173 **cell RNA sequencing**

174 Single cell RNA-seq (scRNA-seq) data of Schwann cells (SCs) differentiated from human
175 amniotic mesenchymal stem cells (hAMSCs) was downloaded from Gene Expression Omnibus
176 (GSE161066) [28]. Seurat [33] was used for initial data cleaning and quality control, removing
177 cells with >2,500 or <200 unique feature counts as well as cells with >5% mitochondrial RNAs.
178 The hAMSC and SCs samples were each normalized with SCTransform [34, 35] and then
179 integrated with Harmony [36, 37]. Uniform manifold approximation and projection (UMAP) [38]
180 was used as a final dimensionality reduction step. The integrated object was clustered, markers
181 were identified for each cluster ($|Log_2FC|>0.58$ and $FDR<0.05$), and the relative cluster
182 proportions were compared between hAMSCs and SCs. DGE analysis was also performed

183 between hAMSC and SCs to identify DEGs specific to either group ($|Log_2FC|>0.58$ and
184 *FDR<0.05*).

185 **Evaluation of Schwann cell differentiation in mouse sciatic nerve**

186 Bulk RNAseq data (FPKM values) from sciatic nerve harvested at various developmental stages
187 (E17.5, P1, P5, P14, P24, P60) and peripheral nerves distal to the DRG at E13.5 were
188 downloaded from the SNAT data portal/GEO (GSE137870) [29]. For gene names with more
189 than one ID, the ID was selected with the highest average expression across all cells in the
190 dataset. Because gene to gene comparisons are biases by sequence length, we converted the
191 FPKM values to TPM values for gene filtering. Genes with a TPM value greater than the median
192 TPM value of all genes were retained for downstream analysis. Next, differential gene
193 expression analysis was performed using edgeR (3.34.1). Six comparisons were performed,
194 one for each timepoint (E17.5, P1, P5, P14, P24, P60) compared to the E13.5 reference
195 timepoint. Genes were considered differentially expressed if they had an $|Log_2FC|>5$ and an
196 *FDR<0.001*. Genes were mapped to their appropriate human homolog using biomaRt (2.48.3)
197 and the Dec 2021 Ensembl archive for both human and mouse.

198 **Evaluation of myelinating compared to non-myelinating mouse Schwann cells**

199 Bulk RNAseq data (FPKM values) from sorted Schwann cell populations enriched for
200 myelinating versus non-myelinating Schwann cells were downloaded from the SNAT data
201 portal/GEO (GSE137947) [29]. The initial processing and homolog mapping steps were as
202 described above. DEGs were compared between myelinating and non-myelinating Schwann
203 cells. Genes were considered differentially expressed if they had an $|Log_2FC|>5$ and an
204 *FDR<0.001*.

205 **Cellular subtyping of Schwann cells from mouse sciatic nerve**

206 The integrated Seurat (4.3.0) object from the SNAT data portal (SS2_all) was downloaded [29]
207 for analysis and comparison with additional datasets. UMAP was calculated on the integrated
208 components using the first 10 dimensions. Marker genes were identified using the
209 FindAllMarkers function. The homolog mapping steps were as previously described. In addition
210 to identifying markers from the previously defined clusters, we also determined DEGs for
211 various differentiation trajectories. Specifically, we identified DEGs using the FindMarkers
212 function contrasting immature Schwann cells (iSCs) from myelinating Schwann cells (mSCs),
213 i.e., iSC vs. tSC and nm(R)SC, and DEGs contrasting iSCs from non-myelinating Schwann cells
214 (nmSCs), i.e., iSC vs. pmSC, mSC cluster 1, mSC cluster 2, and mSC cluster 3. Genes were
215 considered differentially expressed if they had an $|Log_2FC|>0.58$ and an $FDR<0.05$.

216 **Identification of conserved gene expression programs in differentiating Schwann cells**
217 **across myelination status and species**

218 To examine the similarity of transcriptional programs between mouse and hiPSCs during
219 Schwann cell differentiation, we compared DEGs from our SC-IU dataset with the SNAT RNA-
220 seq dataset for each of the six time point comparisons. The Jaccard index (JI) was calculated
221 for up-regulated DEGs for each pairwise comparison between the SC-IU and SNAT datasets
222 (i.e., E17.5 up-regulated DEGs (SNAT) and Day 3 up-regulated DEGs (SC-IU) JI, E17.5 up-
223 regulated DEGs (SNAT) and Day 6 up-regulated DEGs (SC-IU) JI, etc.). The same process was
224 conducted for the down-regulated DEGs, resulting in a total of 36 total JI values for the up-
225 regulated and downregulated DEGs, respectively. We then averaged and normalized the JI
226 values to obtain a square matrix with row and column sums of 1 to account for any skew toward
227 either end of the differentiation process. We then repeated this process with less stringent DEG
228 calling criteria ($|Log_2FC|>0.58$ and an $FDR<0.05$). The consistency of the JI matrix was
229 evaluated using a Student's t-test of the diagonal of the matrix vs. the off-diagonal and a
230 Spearman correlation of the JI with the distance of each cell from the diagonal. Next, we

231 compared the union of up-regulated and down-regulated DEGs from both the SC-IU and SNAT
232 datasets to differentiation and developmental gene modules from the WGCNA analysis using
233 the original criteria ($|Log_2FC|>5$ and an *FDR<0.001*). Finally, mSC markers and nmSC markers
234 from the SNAT scRNA-seq dataset were compared to the mSC DEGs identified from the SNAT
235 myelination bulk RNA-seq dataset. We use these comparisons to evaluate the consistency of
236 genes across modalities, species, myelination status, and analysis technique to identify high-
237 confidence targets for the study of Schwann cell differentiation.

238

239 **RESULTS**

240 **Morphological and immunofluorescence-based validation of hiPSC induced**
241 **differentiation to SPCs and SCs**

242 To confirm robust differentiation of hiPSCs into Schwann cells precursors (SCPs) and
243 subsequently SCs, we performed morphological and immunofluorescence (IF) staining of cells
244 collected at seven timepoints along the hiPSC to SC continuum (**Fig. 1A**, **Table 1**). We
245 observed morphological changes during the differentiation process where the cells exhibited
246 increasing levels of cohesion into aggregates and reduced levels of random arrangements of
247 individual cells (**Fig. 1A**). Schwann cells are derived from the neural crest and characterized by
248 the expression of distinct makers including S100β, p75, HOXb7, and GAP43 (**Fig. 1B**). A
249 gradual increase in the expression of S100β, p75, HOXb7, and GAP43 was observed
250 throughout the differentiation process reaching a maximum at the SC stage (**Fig. 1B, Fig S1**).
251 Collectively, these findings indicate that our methodology can efficiently generate SCPs and
252 SLPs from hiPSC with high fidelity.

253 **Differential gene expression during SC differentiation**

254 To characterize gene expression dynamics during Schwann cell differentiation, we performed
255 RNA sequencing of cells collected at seven discrete stages along the hiPSC to SC continuum.
256 As anticipated, replicates from each stage of differentiation clustered together in PCA space
257 (**Fig. 1C**). Notably, the hiPSC stage had clear separation from all other stages (**Fig. 1C**) and the
258 neural rosette (NR) through SCP stages of differentiation clustered more closely together
259 compared to other stages (**Fig. 1C**). There were considerable transcriptional differences
260 between all stages of differentiation, most notably hiPSCs versus later stages of differentiation
261 (**Fig. 1D, Fig. S1-S3**). We identified 18 genes that were significantly up-regulated across all 6
262 comparisons (**Table 2**). Of these, *ANXA1* and *CDH6* were also among the top 5 most significant
263 up-regulated DEGs (lowest FDR adjusted p-values) within any of the timepoint comparisons
264 (**Table 2**). Notably, *CDH6* is associated with cell-cell adhesion and *ANXA1* has been implicated
265 in Schwann cell proliferation and migration [47]. Of the 30 total top 5 up-regulated DEGs per
266 timepoint comparison, 18 were up-regulated across all timepoints These 18 genes were
267 enriched for ontology terms related to cell adhesion (GO:0007155, $P<0.001$) and anatomical
268 structure formation involved in morphogenesis (GO:0048646, $P<0.001$). In total, 50 significantly
269 down-regulated DEGs were identified at each timepoint comparison (**Table 2**). However, only
270 four were also found in the top 5 most significant down-regulated DEGs (lowest FDR adjusted
271 p-values) at any of the timepoint comparisons (**Table 2**). Of the top 5 down-regulated DEGs per
272 timepoint comparison, 18 genes were down-regulated across all timepoints and were enriched
273 for ontology terms related to the regulation of cell fate specification (GO:0042659, $P<0.001$).

274 **Gene co-expression modules associated with differentiation, axon guidance and ECM**

275 Building on the results of our differential gene expression analysis, we next performed weighted
276 gene co-expression network analysis (WGCNA) to identify co-regulated gene modules during
277 hiPSC differentiation to SCs. WGCNA identified 24 modules (**Fig. 2A**), and 11 of these had
278 significantly altered eigengene values during differentiation (i.e., $P<0.05$, **Table 3**). Of the 11

279 differentiation-associated modules, 10 had significantly enriched ontology terms associated with
280 them (**Table 3**). The most significant module identified by ANOVA was the brown module
281 (*P<0.001*, **Table 3**, **Fig. 2B**) which had an eigengene peak at day 6, i.e., a significant increase
282 from day 3 to day 6 (*P<0.001*, **Fig. 2B**) followed by a decrease from day 6 to day 12 (*P<0.001*,
283 **Fig. 2B**). Given the close relationship between Schwann cell development and neurons, we
284 were intrigued that the brown module was functionally enriched for axon guidance (P<0.001,
285 **Fig. 2C**), forebrain development (*P<0.001*, **Fig. 2C**), and sensory organ morphogenesis
286 (*P<0.001*, **Fig. 2C**).

287 The next two most significant modules were red (*P<0.001*) and turquoise (*P<0.001*) (**Table 3**).
288 The red module eigengene steadily increased from hiPSC to SCP stage (*P<0.001*, i.e., day 0 to
289 day 24, **Fig. S4**) then dramatically decreased from SCP to SC stage (*P<0.001*, i.e., day 24 to
290 day 31, **Fig. S4**) and was functionally enriched for biosynthetic pathways (**Fig. S4**). In contrast,
291 the turquoise module eigengene, which was functionally enriched for functionally enriched for
292 exocytosis (*P<0.001*, **Fig. S5**) and regulation of neuron projection development (*P<0.001*, **Fig.
293 S5**) decreased dramatically from the hiPSC to preneural rosette (pre-NR) stage (*P<0.001*, i.e.,
294 day 0 to day 3, **Fig. S5**) and remained suppressed through terminal SC differentiation (*P=0.732*,
295 i.e., day 3 to day 31, **Fig. S5**). Another pair of modules that showed distinct expression patterns
296 were the pink and blue modules (*P<0.001* and *P<0.001* respectively, **Table 3**). Similar to the
297 brown module that had a distinct eigengene peak at day 6, the pink module peaked at day 12,
298 i.e., a significant increase from day 6 to day 12 (*P<0.001*, **Fig. 2D**) and decreased thereafter
299 from day 12 to day 18 (*P<0.001*, **Fig. 2D**). Not surprisingly, this module had numerous ontology
300 terms related to cell fate commitment and ear development (**Fig. 2E**). The blue module
301 eigengene also had a peak early in hiPSC to SC differentiation at day 3, i.e., a significant
302 increase from day 0 to day 3 (*P<0.001*, **Fig. 2F**) and decrease from day 3 to day 6 (*P<0.001*,
303 **Fig. 2F**). However, this module eigengene gradually increased again from NR through

304 completion of SC maturation (*P<0.001*, **Fig. 2F**). Notably, the blue module contains the *NF2*
305 tumor suppressor gene and had significant functional enrichment for extracellular matrix
306 organization (*P<0.001*, **Fig. 2G**), extracellular structure organization (*P<0.001*, **Fig. 2G**), and
307 cell-substrate adhesion (*P<0.001*, **Fig. 2G**). Taken together with the remaining modules (**Fig.**
308 **S6-S11**), the results of our WGCNA reveal that hiPSC differentiation to SCs is associated with
309 dynamic changes in gene expression that are reflective of Schwann cell biological function and
310 show associations with neural morphology, ear development, and cellular organization.

311 **Signatures of hAMSC to SC differentiation are unique at the single cell level**

312 To evaluate the robustness and generalizability of our findings, we extended our analysis to
313 examine whether similar gene modules and pathways were retained in other complementary
314 models of human Schwann cell differentiation. Wei and colleagues performed single cell RNA-
315 sequencing of SCs derived from human amniotic mesenchymal stem cells (hAMSCs) to identify
316 heterogenous SC populations [28] (SC-SUMC: GSE161066, **Table 1**). The scRNA-seq data
317 contained 3,892 hAMSCs and 1,729 SCs. After quality control (QC) and dimensionality
318 reduction, we identified a total of 16 clusters (**Fig. 3A**). DGE analysis revealed clear differences
319 between hAMSC and SCs. Some of the most upregulated genes in SC compared to hAMSCs
320 included ECM related genes like: *COL1A1* and *COL3A1* (**Fig. 3B**, **Table 4**). To further
321 characterize each cluster, we performed cluster-specific marker analysis using Seurat to identify
322 distinct gene sets highly expressed in each cluster (**Fig. 3C**). We observed that some clusters
323 had a higher proportion of either hAMSCs or SCs, suggesting that they may represent different
324 stages of differentiation **(Fig. 3D**). For example, cluster 8 and 14 comprised of a higher
325 proportion of SC sample compared to the hAMSC sample (**Fig. 3D**) and both of these clusters
326 overexpressed ECM-related markers. Cluster 8 overexpressed *VIM*, and cluster 14
327 overexpressed *ITGA1*, *COL1A1*, and *ADAMTS6* (**Fig. 3C**, **Table S1**).

328 **Evaluation of Schwann cell differentiation in mouse sciatic nerve**

329 To further validate our hiPSC model of Schwann cell differentiation *in vitro*, we further compared
330 our transcriptomic data with an *in vivo* dataset comprehensively cataloging Schwann cell
331 development in the mouse sciatic nerve. Gerber and colleagues generated gene expression
332 profiles from Schwann cells isolated from mouse sciatic nerve throughout embryogenesis and
333 postnatal development, which are publicly available through the Sciatic Nerve Atlas, i.e., SNAT,
334 [29]. By integrating bulk and single cell RNA-seq data from SNAT, we identified unique and
335 conserved gene signatures of Schwann cell differentiation across species and modalities.

336 In our SC-IU dataset, a total of 50 genes were significantly up-regulated across all timepoint
337 comparisons, i.e., were contained in each comparison (**Fig. 4A-F, Table S2, Table S3**). These
338 genes represented myelination (GO:0042552, $P<0.001$) and collagen-containing extracellular
339 matrix (GO:0062023, $P<0.001$). The 362 down-regulated DEGs significant at all comparisons
340 were enriched for neuron development (GO:0048666, $P<0.001$) and synaptic signaling
341 (GO:0099536, $P<0.001$). Furthermore, we identified 9 gene co-expression modules that were
342 significantly altered over developmental stage from E13.5 to P60. (**Table S4**, **Fig. S12-S21**).
343 Notably some of these modules were also enriched for terms related to neural development like
344 the SNAT-brown module (GO:0010975, Regulation of neuron projection development, $P<0.001$,
345 **Table S4**).

346 **Differential gene expression and enrichment in myelinating versus non-myelinating**
347 **murine Schwann cells**

348 We next sought to investigate the gene expression profiles of myelinating (mSCs) and non-
349 myelinating (nmSCs) in the Sciatic Nerve Atlas. mSCs had 478 up-regulated DEGs and 471
350 down-regulated DEGs in comparison to nmSCs (**Fig. 4G, Table S5**). These up-regulated DEGs
351 were enriched for structural constituents of myelin sheath (GO:0019911, $P=0.039$), myelination

352 (GO:0042552, *P<0.001*), and sterol biosynthetic processes (GO:0016126, *P<0.001*). Down-
353 regulated DEGs were highly enriched for mitotic cell cycle (GO:0000278, *P<0.001*), cell division
354 (GO:0051301, *P<0.001),* and positive regulation of cell cycle processes (GO:0090068,
355 *P<0.001*).

356 The myelinating and non-myelinating Schwann cell subsets remained largely distinct even upon
357 recomputing the UMAP dimensionality reduction (**Fig. 5A**)[29]. Two distinct trajectories
358 emerged, both beginning from proliferating Schwann cells (prol. SC) and terminating at either
359 mSC cluster 3 or nm(R)SC (**Fig. 5A**)[29]. We observed 261 up-regulated and 116 down-
360 regulated DEGs in myelinating Schwann cells (mSC) as compared to immature Schwann cells
361 (iSCs) (**Table S6**). As expected, the up-regulated DEGs in mSCs were enriched for terms
362 related to regulation of nervous system development (GO:0051960, *P<0.001*) and myelination
363 (GO:0042552, *P<0.001*). However, the most significantly enriched term was sterol biosynthetic
364 process (GO:0016126, *P<0.001*). The robust upregulation of cell cycle inhibitors like *CDKN1A*
365 (**Fig. 5B**) in conjunction with the downregulation of cyclins such as *CDK6* (**Fig. 5B**) further
366 suggest a state of proliferative arrest within this cluster. Using as few as three transcriptomic
367 markers, we could distinguish the stages of Schwann cell differentiation and the bifurcation of
368 mSCs and nmSCs (**Fig. 5C & D, Table S7**). Again, we identified ECM-related markers in the
369 different differentiation stage iSC (*POSTN*), tSC (*ID3*), and mSC (*SPP1*) clusters (**Table S7**).

370 **Differentiating Schwann cells have conserved pathways related to ECM**

371 As anticipated, the transcriptional signatures of Schwann cell differentiation were not identically
372 conserved between hiPSCs and mice, likely due to both species and model specific differences.
373 Without normalization, there was no significant correlation between the developmental stages
374 within the SNAT dataset and the iPSC differentiation timepoints (**Fig. S22**). However, after
375 accounting for differences in the row and column DEG counts, a moderate association emerged

376 (PCC=0.44, *P=0.007*, **Fig 6A**). The one-to-one correspondences in DEGs between timepoints
377 (E17.5-Day 3, P1-Day 6, P5-Day 12, P14-Day 18, P24-Day 24, and P60-Day 31) were also
378 moderately associated (*P=0.084*, **Fig. 6B**).

379 We focused on the blue module and turquoise modules and compared them to the up- and
380 down-regulated DEGs from the SC-IU and SNAT datasets. The blue module contained *NF2*
381 and the eigengene trended upward throughout the differentiation process, whereas the
382 turquoise module trended downward. We found that the up-regulated DEGs from both SC-IU
383 and SNAT had high overlap with the blue module, but low overlap with one another (**Fig. 6C**). In
384 contrast the SC-IU up-regulated DEGs had lower overlap with the turquoise module, while
385 SNAT up-regulated DEGs had a similar number of DEGs in the turquoise module (**Fig. 6D**).
386 Both the SC-IU and SNAT down-regulated DEGs had lower overlap with the blue module (**Fig.**
387 **6E**) than with the turquoise module (**Fig. 6F**). Notably 21 genes were up-regulated in both
388 datasets and contained within the blue module (**Table S2**). These genes represented specific
389 molecular functions including extracellular matrix structural constituent (GO:0005201, *P=0.005*)
390 and S100 protein binding (GO:0044548, *P=0.008*) as well as biological processes including
391 caveola assembly (GO:0070836, *P=0.006*) and regulation of transforming growth factor beta
392 receptor signaling pathway (GO:0017015, *P=0.006*).

393 In addition to these unique conserved processes during murine Schwann cell development and
394 hiPSC to Schwann cell differentiation, mSCs had distinct molecular profiles in comparison to
395 nmSCs that were recapitulated in both RNA-seq and scRNA-seq data modalities. Notably, mSC
396 up-regulated DEGs from SNAT RNA-seq had high overlap with mSC markers from SNAT
397 scRNA-seq (**Fig. 6G**). Similarly, nmSC up-regulated DEGs from SNAT RNA-seq exhibited a
398 high degree of overlap with nmSC markers from SNAT scRNA-seq (**Fig. 6H**).

399 **DISCUSSION**

400 We have developed a state-of-the-art platform to study Schwann cell development using
401 hiPSCs. We demonstrate that hiPSCs successfully differentiated into SCs based on marker
402 gene expression and morphology. Furthermore, we identify similar transcriptomic profiles in our
403 hiPSC to SC differentiation model as observed in other external Schwann cell differentiation
404 studies [28, 29]. Notably, we observed correlation of DEGs and gene expression signatures
405 including those relating to ECM and TGF-β signaling between hiPSC derived SCs and those
406 arising in situ from the developing mouse sciatic nerve [29]. Intriguingly, TGF-β1 signaling has
407 been shown to coordinate the production of abundant ECM proteins by *Nf1* deficient Schwann
408 cells, contributing to plexiform neurofibroma pathogenesis in neurofibromatosis type 1 (NF1)
409 [39]. However, the role of ECM and TGF- β signaling in schwannoma development remains
410 largely understudied.

411 Key differences between our hiPSC model and mouse Schwann cell development also
412 emerged, which may be attributable to both species-specific differences as well as the model
413 system employed (*in vitro* versus *in vivo*). Transcriptional discordance between SCs derived
414 from hAMSCs versus hiPSCs may in part be attributable to unique cells of origin and the
415 experimental differences related the reprograming process. While hiPSCs have been utilized
416 successfully to overcome limitation of mouse models to enhance our understanding of
417 psychiatric disorders [40] and Alzheimer's disease [21], further investigation is needed to
418 validate the fidelity of this platform in recapitulate the pathogenesis of *NF2*-SWN and other
419 Schwann cell associated disorders.

420 Notwitstanding these disparities, our analysis did reveal distinctive gene signatures associated
421 with Schwann cell development that were conserved across species and model systems. We
422 identified gene co-expression modules related to differentiation, particularly the 'blue module'
423 that contained the *NF2* tumor suppressor gene. This module demonstrated functional
424 enrichment for multiple terms related to ECM and actin filaments, which is consistent with the

425 established relationship between Merlin and F-actin dependent cytoskeletal defects in *NF2*-
426 associated schwannoma [41]. The emergence of ECM-related genes was a consistent finding
427 across datasets, analytical techniques, and experimental methodologies employed in the study
428 of differentiating Schwann cells. Notably, two vesicle-associated genes within the 'blue module',
429 *CAV1* and *CAV2*, were found to be upregulated in both hiPSC and murine derived SCs and
430 recently *NF2* was shown to regulate vesicle trafficking in schwannoma [42]. Additionally,
431 collagens *COL1A1* and *COL3A1*, were also overrepresented in our analysis and recently shown
432 to be associated with recurrence of vestibular schwannoma after radiation therapy [43]. Other
433 ECM-related genes identified, albeit with lesser substantiation in schwannoma included *ITGA1*,
434 *POSTN*, *SPP1*, *ID3*, and *ADAMTS6*. One of the most promising candidates was lysyl oxidase,
435 i.e., *LOX*, which recurred in multiple analyses. LOX is an essential protein in the ECM that
436 mediates conversion of collagen precursors into reactive forms capable of cross-linking and
437 stabilizing ECM proteins to modulate cell adhesion and motility [44].

438 Cell cycle inhibitors, such as *CDKN2B*, were also present in the 'blue module' and conserved in
439 cross species analysis. *CDKN2B* is a key component of the *INK4/ARF* tumor suppressor locus
440 and can induce proliferation when deleted or mutated in a multitude of cancer types [45, 46].
441 Furthermore, we identified hiPSC-specific genes of interest that were highly up-regulated during
442 SC differentiation and differentially expressed at all timepoints including *ANXA1,* which has
443 been implicated in promoting Schwann cell proliferation and migration in response to nerve
444 injury [47], yet its relationship to Merlin in Schwann cell biology remains unknown.

445 In summary, we developed a novel hiPSC Schwann cell differentiation model and performed
446 integrated analyses across five datasets from three independent studies, encompassing both
447 scRNA-seq and RNA-seq. Our findings indicate that our hiPSC model robustly recapitulates
448 Schwann cell ontologies and identifies critical genes implicated in Schwann cell differentiation
449 warranting further investigation. Additionally, our data revealed a pronounced association

450 between SC development and ECM across multiple datasets, that remains largely
451 uncharacterized with respect to Merlin biology and schwannoma development. Future studies
452 leveraging this hiPSC platform to conduct CRISPR-Cas9 editing of *NF2* and other associated
453 genes relevant to SC differentiation/function, generate hiPSC organoid co-cultures, and perform
454 bulk and single cell mulitomic analysis hold promise to reveal new insights into Schwann cell
455 biology, the Schwann cell-ECM relationship, and schwannomas pathogenesis in *NF2*-SWN.

456 **ACKNOWLEDGEMENTS**

457 We would like to acknowledge the help and support of the Indiana University School of Medicine
458 Center of Computational Biology and Bioinformatics, the Indiana University Information
459 Technology Services for their high-performance computing resources, and the Indiana
460 Biosciences Research Institute for their lab space and technical support.

461
462 **FUNDING**
463
464 Funding from the Indiana Biosciences Research Institute to A.S. and T.S.J., 1R21CA264339 to
465 T.S.J. S.D.R. is supported by the Francis S. Collins Scholars Program in Neurofibromatosis
466 Clinical and Translational Research funded by the Neurofibromatosis Therapeutic Acceleration
467 Program (NTAP, 2004757180), a K08 Mentored Clinical Scientist Research Career
468 Development Award funded by the NIH/National Institute of Neurological Disorders and Stroke
469 (NINDS) (K08-NS128266-02), and startup funding from the Department of Pediatrics at the
470 Indiana University (IU) School of Medicine and the IU Simon Comprehensive Cancer Center
471 (IUSCCC).

472
473 **DISCLOSURES**
474
475 O.L., W.C., A.H., A.Q., T.S.J., are partially supported by the Indiana Biosciences Research
476 Institute. A.H. currently holds a research position at Eli Lilly and Company.

477
478 **AUTHOR CONTRIBUTIONS**

S.D.R, A.S.Q, and T.J. designed the experiments and evaluated the data. W.C, A.H, A.S.Q, and B.E.H. performed the experiments. O.L, S.L, and T.J analyzed all data and prepared the graph. T.J, S.L, A.S.Q, and S.D.R wrote the initial draft of the manuscript. S.P.A and D.W.C. gave advice during the project achievement. All co-authors provided feedback and revisions.

484 **TABLES**

485 **Table 1** Table of datasets used for analysis in this study

Dataset name	Samples	Description	Publication	PMID	Accession
SC-IU	21 samples RNA-seq (3 replicates across 7 timepoints) RNA-seq	hiPSC to SC differentiation sampled at seven timepoints Organism: Human	This study	This study	This study
SC-SUMC	2 samples (1 hAMSC sample with 3,892 cells and 1 SC sample with 1,729 cells) scRNA-seq	hAMSC to SC differentiation sampled at hAMSC and SC stages Organism: Human	Wei, Z. frontiers in Physiology. (2021)	34093220	GSE161066
SNAT	28 samples (4 replicates across 7 timepoints) RNA-seq; 8 FACS samples (4 mSC and 4 nmSC) RNA-seq; 8 samples (2 replicates across 4 stages: P1, P5, P14, and P60) scRNA-seq	SCP to SC differentiation; Comparison of mSC and nmSCs; Cellular subtyping of Schwann cells during stages of development. Organism: Mouse	Gerber, D. eLife. (2021)	33890853	GSE137870

486

487 **Table 2** Top 5 up- and down-regulated DEGs for each of the 6 timepoints (k) (days 3, 6, 12, 18,

488 24, and 31) compared to day 0 hiPSCs as the reference.

Day k vs. Day 0	Gene	Log2FC	P	FDR
Day 3 Up	*COL8A1*	11.33	0	0
Day 3 Up	*POSTN*	10.15	0	0
Day 3 Up	*SERPINE1*	9.22	0	0
Day 3 Up	*IGFBP3*	7.61	0	0
Day 3 Up	*TGFBI*	7.15	0	0
Day 3 Down	*CD24*	-6.37	5.14E-260	8.69E-257
Day 3 Down	*EPCAM*	-7.93	1.19E-229	1.07E-226
Day 3 Down	*HLA-A*	-5.53	5.65E-213	4.16E-210
Day 3 Down	*PMEL*	-7.55	7.08E-213	5.08E-210
Day 3 Down	*ESRG*	-9.76	7.22E-212	5.06E-209
Day 6 Up	*HAPLN1*	6.97	8.78E-236	2.53E-231

Day 6 Up	*CDH6*	5.91	1.68E-227	2.43E-223
Day 6 Up	*PRTG*	4.91	4.72E-225	4.54E-221
Day 6 Up	*WLS*	5.36	1.57E-184	7.55E-181
Day 6 Up	*GREB1L*	6.90	2.12E-183	8.73E-180
Day 6 Down	*TDGF1*	-5.01	8.98E-198	6.47E-194
Day 6 Down	*ADCY2*	-6.77	1.89E-190	1.09E-186
Day 6 Down	*LINC00678*	-5.15	2.72E-151	7.83E-148
Day 6 Down	*AC064802.1*	-4.65	9.03E-148	2.37E-144
Day 6 Down	*DUSP6*	-4.65	7.95E-145	1.64E-141
Day 12 Up	*ANXA1*	10.95	4.31E-276	6.09E-272
Day 12 Up	*CPE*	5.72	2.35E-191	1.67E-187
Day 12 Up	*PLK2*	5.42	1.95E-190	1.11E-186
Day 12 Up	*PRTG*	4.52	1.72E-185	8.13E-182
Day 12 Up	*CDH6*	5.53	4.22E-181	1.71E-177
Day 12 Down	*TDGF1*	-8.16	0	0
Day 12 Down	*AC064802.1*	-8.52	7.05E-207	6.65E-203
Day 12 Down	*NANOG*	-7.30	7.96E-173	2.82E-169
Day 12 Down	*USP44*	-5.13	5.67E-164	1.46E-160
Day 12 Down	*AC009446.1*	-7.39	2.73E-162	6.42E-159
Day 18 Up	*ANXA1*	10.79	0	0
Day 18 Up	*COL8A1*	10.92	0	0
Day 18 Up	*CAV1*	6.12	0	0
Day 18 Up	*SERPINE1*	8.14	5.48E-295	3.85E-291
Day 18 Up	*POSTN*	8.01	2.79E-294	1.56E-290
Day 18 Down	*TDGF1*	-10.73	2.01E-273	7.06E-270
Day 18 Down	*USP44*	-5.52	1.62E-253	4.54E-250
Day 18 Down	*ZSCAN10*	-6.42	3.59E-216	4.03E-213
Day 18 Down	*ESRG*	-5.16	8.92E-199	7.82E-196
Day 18 Down	*VSNL1*	-7.28	3.70E-179	2.16E-176
Day 24 Up	*ANXA1*	11.19	0	0
Day 24 Up	*POSTN*	8.43	0	0
Day 24 Up	*CAV1*	6.16	0	0
Day 24 Up	*PLK2*	5.77	0	0
Day 24 Up	*SPP1*	4.22	1.63E-291	9.33E-288
Day 24 Down	*USP44*	-5.49	8.04E-274	2.29E-270
Day 24 Down	*ESRG*	-5.53	8.55E-249	1.22E-245
Day 24 Down	*ZSCAN10*	-7.03	1.28E-236	1.52E-233
Day 24 Down	*PMEL*	-4.70	6.92E-211	6.17E-208
Day 24 Down	*B3GNT7*	-6.79	7.86E-201	5.98E-198

Day 31 Up	*CTGF*	6.05	0	0
Day 31 Up	*VIM*	6.55	0	0
Day 31 Up	*COL5A2*	7.04	0	0
Day 31 Up	*COL8A1*	11.75	0	0
Day 31 Up	*POSTN*	9.95	0	0
Day 31 Down	*CD24*	-6.94	0	0
Day 31 Down	*HLA-A*	-6.02	8.07E-296	7.22E-293
Day 31 Down	*SFRP2*	-5.66	3.19E-289	2.61E-286
Day 31 Down	*L1TD1*	-5.78	4.22E-275	3.26E-272
Day 31 Down	*EPCAM*	-7.92	1.74E-267	1.18E-264

Table 3 Significantly altered gene modules in relation to timepoint evaluated by ANOVA. The number of genes in the module, ANOVA P, and most significant GO term are listed for each module. Modules with no significant GO terms are blank.

Module	Genes	P	Top GO term	File
Brown	1449	7.66E-17	Axon guidance	File S2
Red	845	2.63E-14	Organic hydroxy compound biosynthetic process	File S3
Turquoise	4615	5.23E-14	Nuclear chromosome segregation	File S4
Cyan	100	1.38E-11		File S5
Pink	692	2.11E-11	Cell fate commitment	File S6
Blue	3797	2.16E-10	Extracellular matrix organization	File S7
Black	833	1.73E-8	Intraciliary transport particle B	File S8
Magenta	159	4.99E-5	Endoplasmic reticulum protein-containing complex	File S9
Yellow	1288	1.52E-2	Cytoplasmic translation	File S10
Midnight Blue	78	4.19E-2	Transcription coregulator activity	File S11
Green Yellow	146	4.26E-2	Methyltransferase activity	File S12

Table 4 Top 10 up- and down-regulated DEGs in hAMSCs versus SCs from the SC-SUMC dataset.

Gene	Proportion hAMSCs>0	Proportion SCs>0	Log_2FC	P	FDR
ISG15	0.04	0.44	0.66	1.00E-300	0.00E+00
IFI27	0.02	0.32	0.61	4.98E-256	5.71E-252
IFI6	0.01	0.27	0.45	1.37E-210	1.58E-206
COL3A1	0.07	0.40	0.55	2.62E-202	3.00E-198
COL1A1	0.06	0.34	0.49	6.85E-174	7.86E-170

LGALS1	0.49	0.81	0.68	2.36E-171	2.71E-167
EEF1A1	0.97	0.88	-0.58	1.66E-158	1.90E-154
BST2	0.02	0.22	0.34	1.86E-139	2.14E-135
TPT1	0.96	0.88	-0.55	1.79E-133	2.05E-129
TPM1	0.31	0.60	0.61	1.85E-118	2.12E-114
TMSB10	0.88	0.95	0.47	2.17E-99	2.49E-95
S100A6	0.47	0.70	0.55	3.15E-99	3.62E-95
RPL3	0.83	0.66	-0.45	8.45E-81	9.70E-77
CXCL8	0.71	0.48	-0.55	9.51E-79	1.09E-74
IGF2	0.20	0.01	-0.34	6.67E-76	7.65E-72
RPS3A	0.80	0.61	-0.42	1.52E-72	1.75E-68
SAT1	0.35	0.12	-0.37	7.64E-72	8.77E-68
MT2A	0.98	0.98	-0.58	1.37E-70	1.57E-66
RPS12	0.89	0.77	-0.40	1.54E-70	1.77E-66
RPS6	0.76	0.57	-0.40	6.27E-67	7.20E-63

496

FIGURES

A

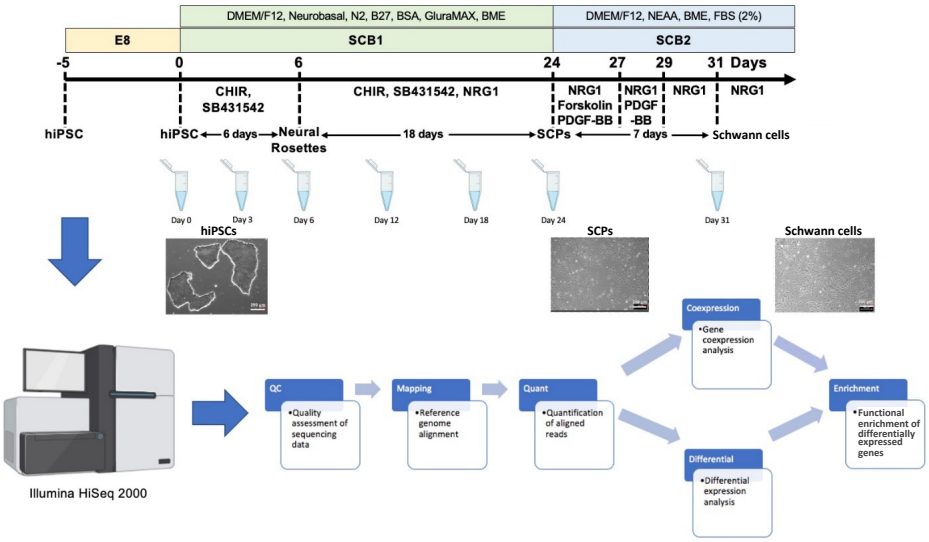

B

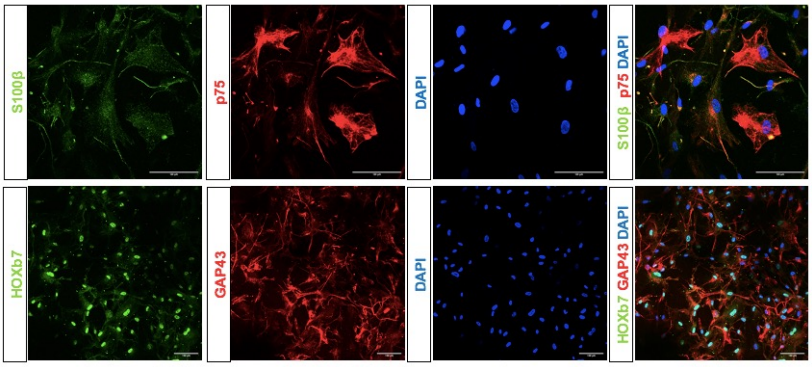

C

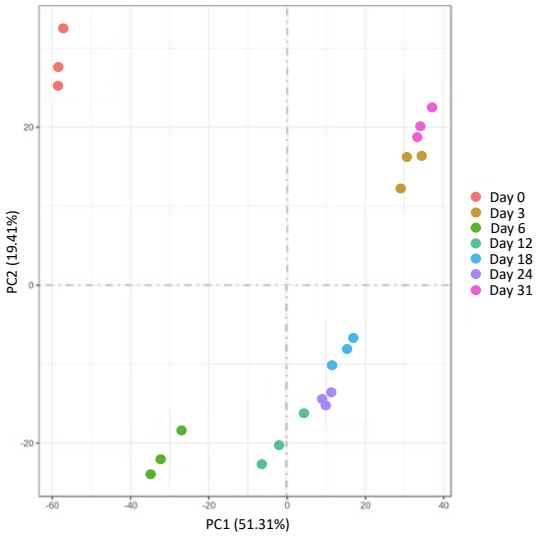

D

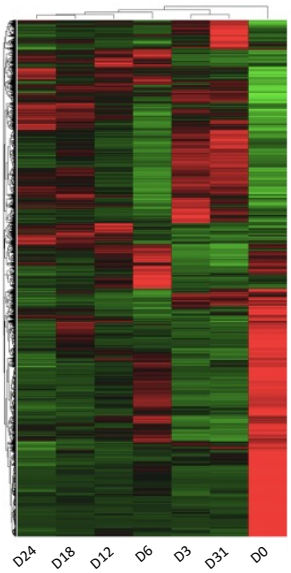

Fig. 1 Workflow and validation of directed differentiation of hiPSCs into human Schwann cells. **A)** Schematic representation of the differentiation of hiPSCs into Schwann cell precursors (SCPs) and Schwann cells (SCs) (Upper panel). Representative bright-field images showing the process of differentiation into SCPs and SCs. Scale bar, 100 µm (middle panel). Steps involve sequencing and data analysis (lower panel). **B)** Schwann cell differentiation was confirmed by positive immunocytochemical staining for S100β (green), p75 (red) in upper panel and HOXb7 (green), GAP43 (red) in lower panel after 31 days of differentiation. DAPI (blue) was used to stain the cell nuclei. Scale bars, 100 µm. **C)** Timepoints can be stratified into stages of differentiation by PCA. **D)** Heatmap of differentially expressed genes across different timepoints where the rows (genes) were clustered using hierarchical clustering.

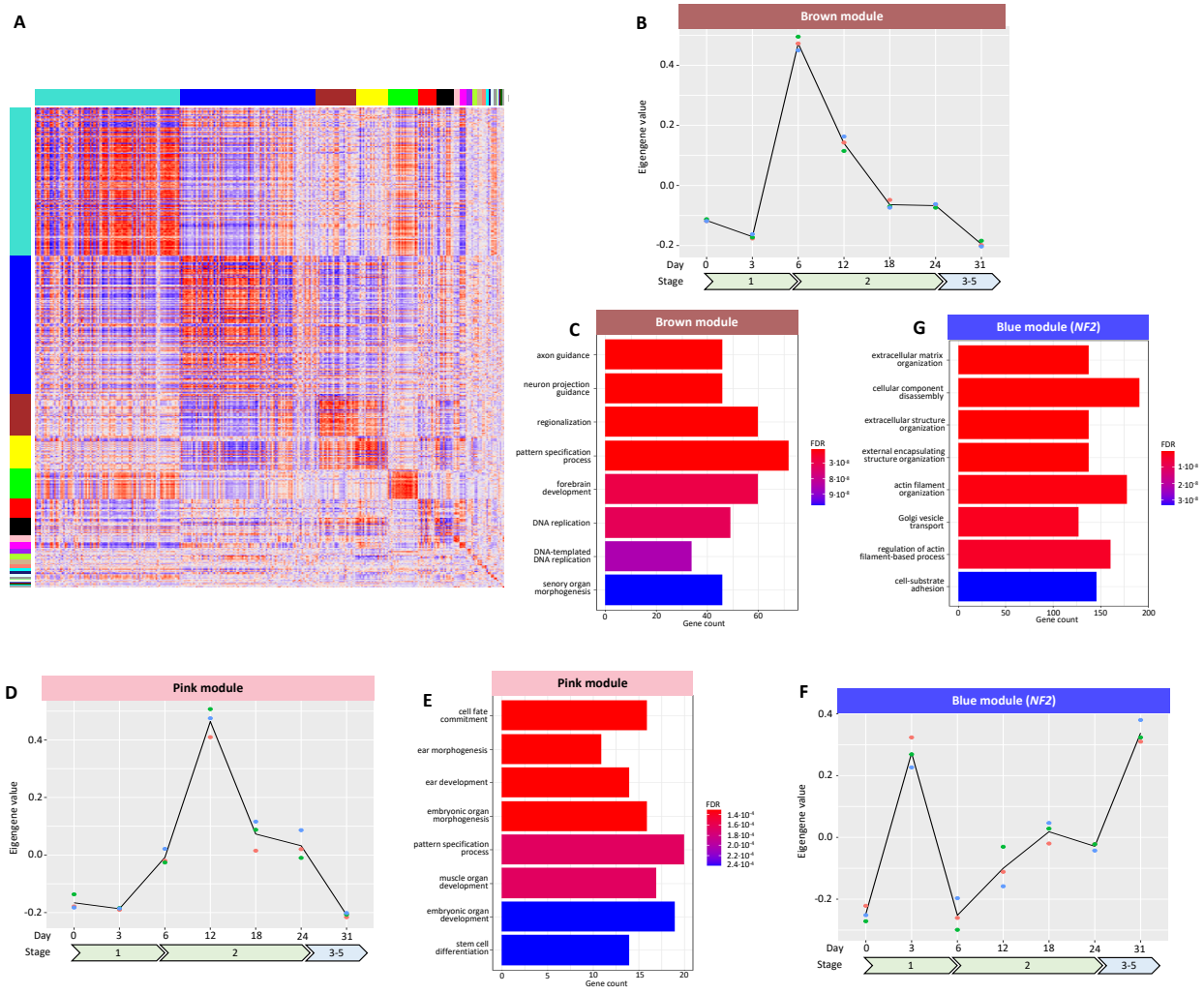

510 **Fig. 2 WGCNA reveals d**ynamic changes in module eigengene values during hiPSC to SC
511 differentiation related to tissue structure and neural development. **A)** Gene correlation matrix
512 with different modules annotated. **B)** Brown module eigengene values are plotted over the
513 course of the study timepoints. **C)** Significant ontology terms from functional enrichment
514 analysis for the brown module. **D)** Pink module eigengene changes over the study timepoints.
515 **E)** Significant ontology terms from functional enrichment analysis for the pink module. **F)** Blue
516 module (containing *NF2*) eigengene changes over the study timepoints. **G)** Significant ontology
517 terms from functional enrichment analysis for the blue module (containing *NF2*).

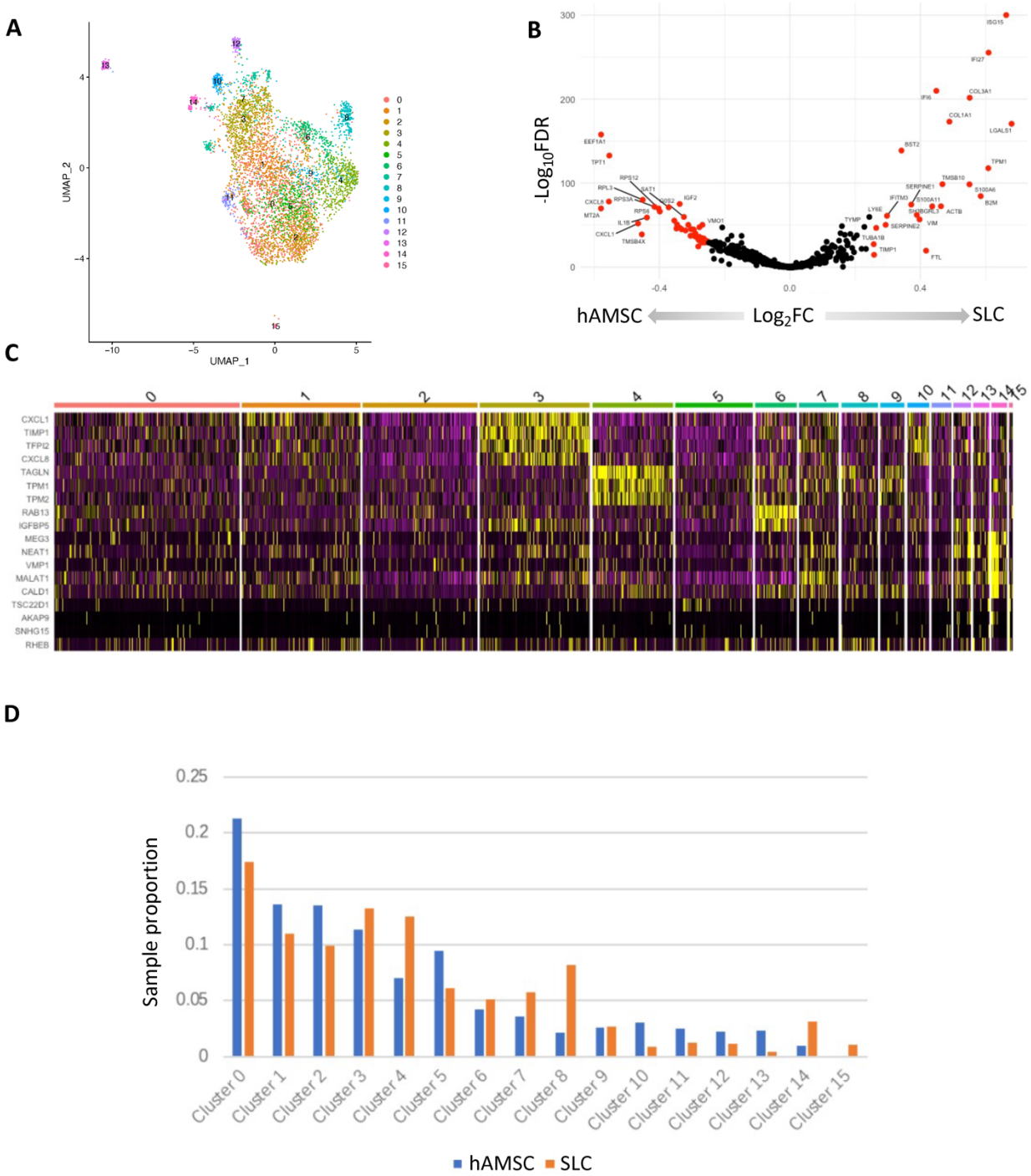

Fig. 3 SC-SUMC scRNA-seq analysis. **A)** UMAP clustering of hAMSCs and SCs from the integrated SC-SUMC dataset (GSE161066) reveals 16 clusters. **B)** Volcano plot of differentially expressed genes when compared between hAMSCs and SCs. **C)** Heatmap of cluster specific

522 markers. **D)** Proportion of hAMSCs and SCs comprising each cluster from the integrated SC-

523 SUMC dataset.

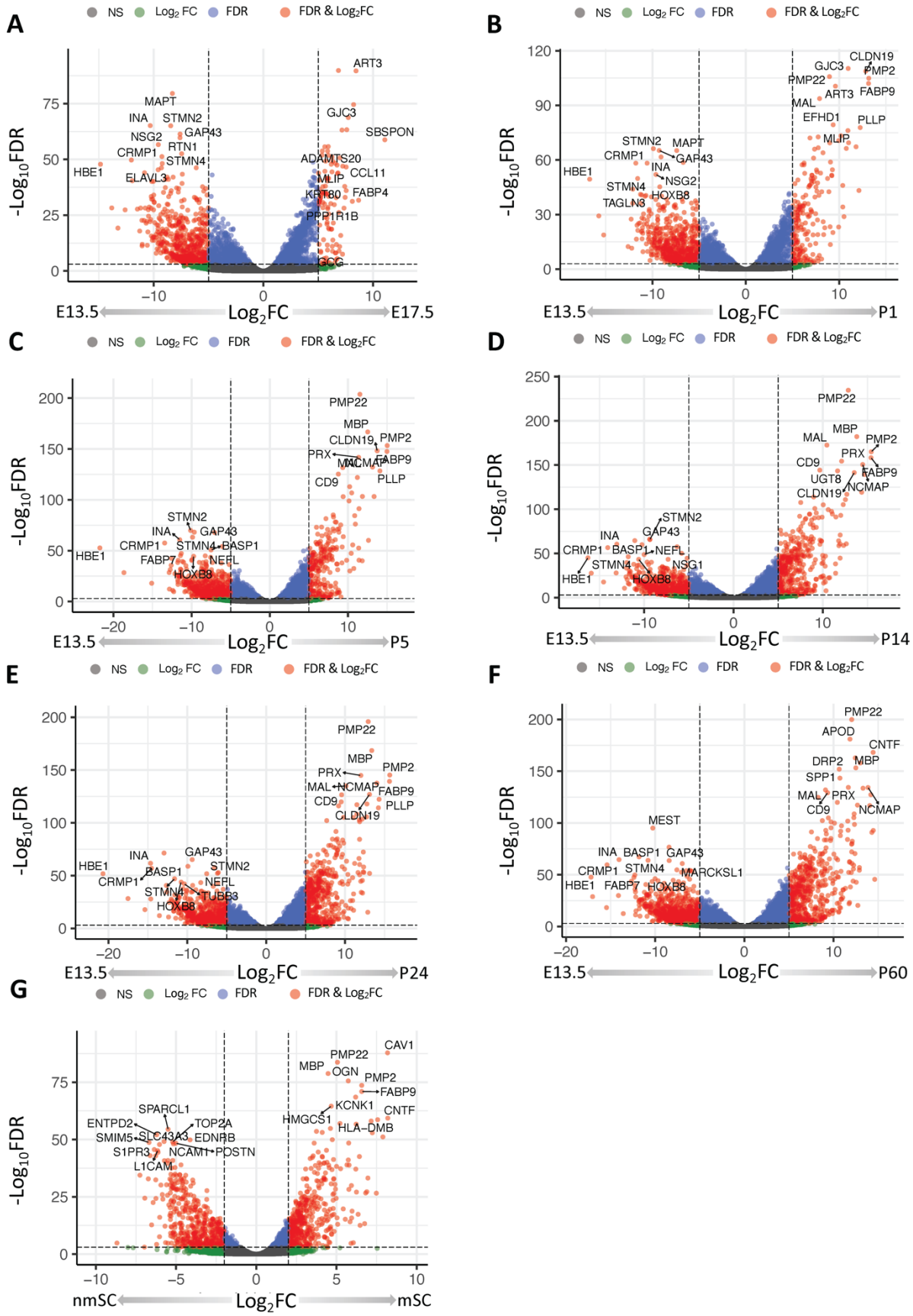
A
NS
Log2 FC
FDR
FDR & Log2FC
-Log10FDR
ART3
MAPT
INA
STMN2
GAP43
NSG2
RTN1
CRMP1
STMN4
HBE1
ELAVL3
GJC3
SBSPON
ADAMTS20
CCL11
MLIP
KRT80
FABP4
PPP1R1B
GCG
E13.5
Log2FC
E17.5
B
CLDN19
GJC3
PMP2
PMP22
ART3
FABP9
MAL
EFHD1
PLLP
MLIP
STMN2
MAPT
CRMP1
GAP43
INA
NSG2
HBE1
STMN4
HOXB8
TAGLN3
P1
C
PMP22
MBP
CLDN19
PMP2
PRX
MAL
NCMAP
FABP9
CD9
PLLP
STMN2
INA
GAP43
CRMP1
STMN4
BASP1
HBE1
FABP7
NEFL
HOXB8
P5
D
PMP22
MAL
MBP
PMP2
CD9
PRX
FABP9
UGT8
NCMAP
CLDN19
STMN2
INA
GAP43
CRMP1
BASP1
NEFL
STMN4
NSG1
HBE1
HOXB8
P14
E
PMP22
MBP
PRX
PMP2
MAL
NCMAP
FABP9
CD9
PLLP
CLDN19
INA
GAP43
HBE1
BASP1
STMN2
CRMP1
NEFL
STMN4
TUBB3
HOXB8
P24
F
PMP22
APOD
CNTF
DRP2
MBP
SPP1
MAL
PRX
CD9
NCMAP
MEST
INA
BASP1
GAP43
CRMP1
STMN4
MARCKSL1
HBE1
FABP7
HOXB8
P60
G
CAV1
PMP22
MBP
OGN
PMP2
FABP9
KCNK1
CNTF
HMGCS1
HLA-DMB
SPARCL1
ENTPD2
TOP2A
SMIM5
SLC43A3
EDNRB
S1PR3
NCAM1
POSTN
L1CAM
nmSC
mSC

524

525 **Fig. 4** Differentially expression analysis of the SNAT RNA-seq dataset (GSE137868). Volcano
526 plots depicting differentially expressed genes when comparing the E17.5 **(A)**, P1 **(B)**, P5 **(C)**,
527 P14 **(D)**, P24 **(E)**, and P60 **(F)** stages to E13.5. Volcano plot depicting differentially expressed
528 genes when comparing myelinating vs. non-myelinating Schwann cells **(G)**.

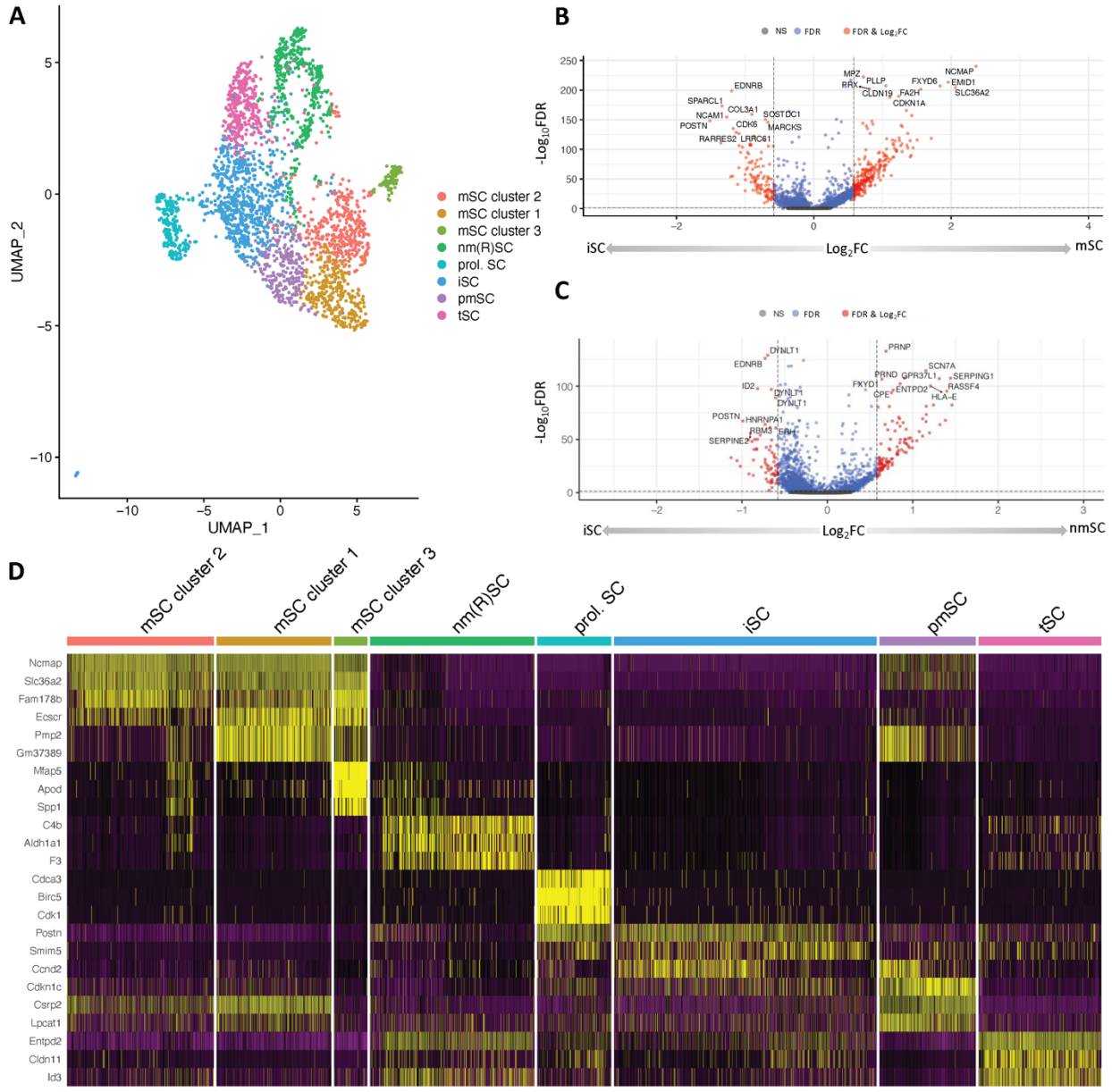

529

530 **Fig. 5** SNAT scRNA-seq analysis. **A)** Scatterplot of 8 clusters identified from the SNAT study
531 representing different stages of Schwann cell development along both myelinating and non-
532 myelinating trajectories. **B)** Volcano plot depicting differentially expressed genes comparing

533 mSC vs iSC. **C)** Volcano plot depicting differentially expressed genes between nmSC versus

534 iSC. **D)** Heatmap of cluster specific markers (top 3).

535

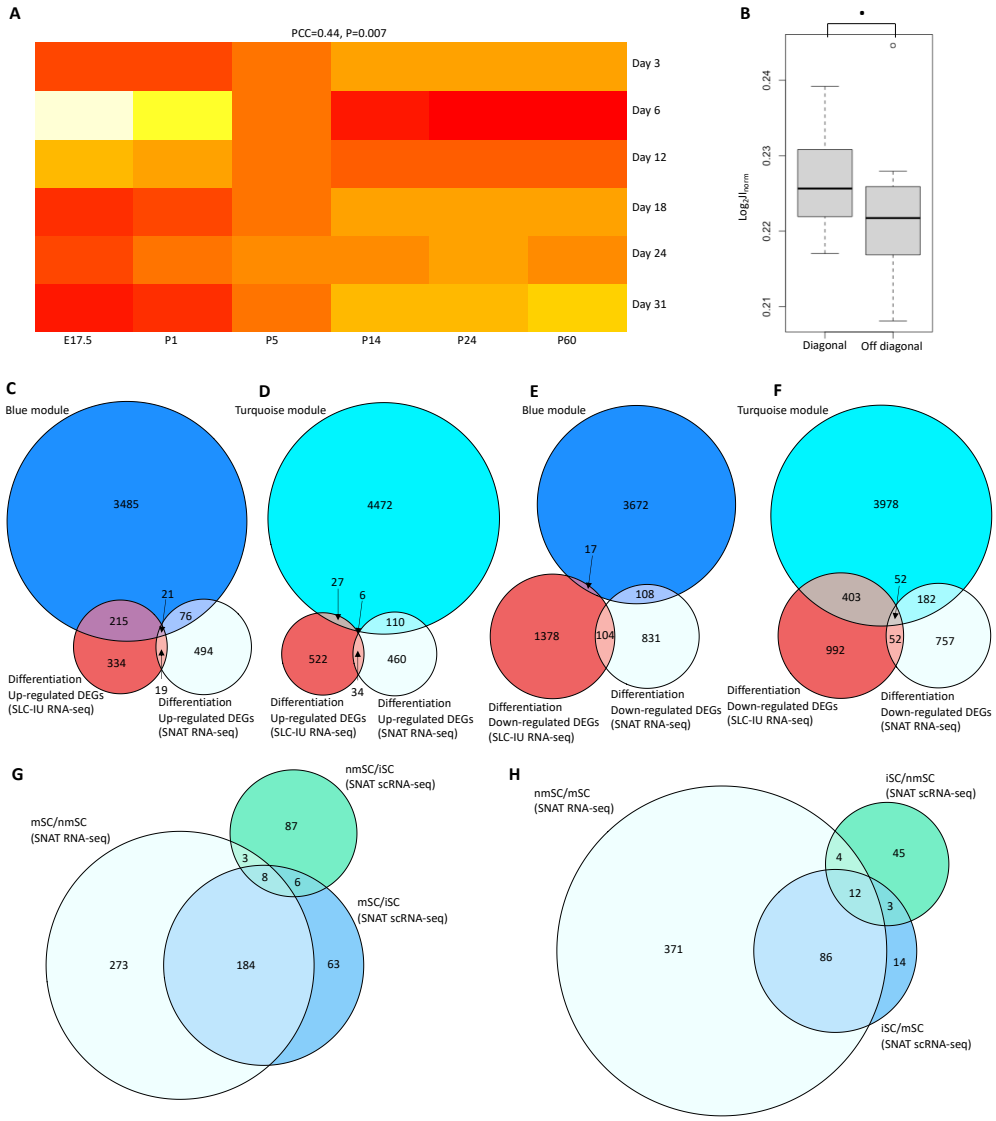

536

537 **Fig. 6** Comparison of DEGs identified between multiple datasets. **A)** Normalized JI matrix of

538 averaged SC-IU DEGs ($|\log_2 FC| > 0.58$ and FDR < 0.05) throughout SC differentiation and

539 SNAT DEGs ($|\log_2 FC| > 0.58$ and FDR < 0.05) through various embryonic and postnatal

540 developmental states with comparison of the JI matrix diagonal to the non-diagonal **(B)**, **C)**

541 Venn diagram comparing genes comprising the blue module, SC-IU up-regulated DEGs during
542 SC differentiation, and SNAT up-regulated DEGs throughout development, **D)** Venn diagram
543 comparing genes comprising the turquoise module, SC-IU up-regulated DEGs during SC
544 differentiation, and SNAT up-regulated DEGs throughout development, **E)** Venn diagram
545 comparing genes comprising the blue module, SC-IU down-regulated DEGs during SC
546 differentiation, and SNAT down-regulated DEGs throughout development, **F)** Venn diagram
547 comparing genes comprising the turquoise module, SC-IU down-regulated DEGs during SC
548 differentiation, and SNAT down-regulated DEGs throughout development, **G)** Comparison of
549 genes up-regulated in mSC vs. iSC and nmSC vs. iSC from SNAT scRNA-seq and DEGs
550 upregulated in mSC vs. nmSC from SNAT RNA-seq, **H)** Comparison of genes down-regulated
551 in mSCs vs. and nmSC vs. iSC from SNAT scRNA-seq and DEGs down-regulated in mSC vs.
552 nmSC from SNAT RNA-seq.
553
554

555 **REFERENCES**

556 1. Jessen, K.R., R. Mirsky, and A.C. Lloyd, *Schwann Cells: Development and Role in Nerve Repair.*
557 Cold Spring Harb Perspect Biol, 2015. **7**(7): p. a020487.
558 2. Salzer, J.L. and B. Zalc, *Myelination.* Curr Biol, 2016. **26**(20): p. R971-R975.
559 3. Goncalves, N.P., et al., *Schwann cell interactions with axons and microvessels in diabetic*
560 *neuropathy.* Nat Rev Neurol, 2017. **13**(3): p. 135-147.
561 4. Carlson, M.L. and M.J. Link, *Vestibular Schwannomas.* N Engl J Med, 2021. **384**(14): p. 1335-
562 1348.
563 5. Evans, D.G., *Neurofibromatosis type 2 (NF2): a clinical and molecular review.* Orphanet J Rare Dis,
564 2009. **4**: p. 16.
565 6. Agnihotri, S., et al., *The genomic landscape of schwannoma.* Nat Genet, 2016. **48**(11): p. 1339-
566 1348.
567 7. Rouleau, G.A., et al., *Alteration in a new gene encoding a putative membrane-organizing protein*
568 *causes neuro-fibromatosis type 2.* Nature, 1993. **363**(6429): p. 515-21.
569 8. Evans, D.G., et al., *A clinical study of type 2 neurofibromatosis.* Q J Med, 1992. **84**(304): p. 603-
570 18.
571 9. Leventoux, N., et al., *Human Astrocytes Model Derived from Induced Pluripotent Stem Cells.*
572 Cells, 2020. **9**(12).
573 10. Perriot, S., et al., *Differentiation of functional astrocytes from human-induced pluripotent stem*
574 *cells in chemically defined media.* STAR Protoc, 2021. **2**(4): p. 100902.
575 11. Perriot, S., et al., *Human Induced Pluripotent Stem Cell-Derived Astrocytes Are Differentially*
576 *Activated by Multiple Sclerosis-Associated Cytokines.* Stem Cell Reports, 2018. **11**(5): p. 1199-
577 1210.
578 12. Voulgaris, D., P. Nikolakopoulou, and A. Herland, *Generation of Human iPSC-Derived Astrocytes*
579 *with a mature star-shaped phenotype for CNS modeling.* Stem Cell Rev Rep, 2022. **18**(7): p. 2494-
580 2512.
581 13. Abud, E.M., et al., *iPSC-Derived Human Microglia-like Cells to Study Neurological Diseases.*
582 Neuron, 2017. **94**(2): p. 278-293 e9.
583 14. Hasselmann, J. and M. Blurton-Jones, *Human iPSC-derived microglia: A growing toolset to study*
584 *the brain's innate immune cells.* Glia, 2020. **68**(4): p. 721-739.
585 15. McQuade, A., et al., *Development and validation of a simplified method to generate human*
586 *microglia from pluripotent stem cells.* Mol Neurodegener, 2018. **13**(1): p. 67.
587 16. Autar, K., et al., *A functional hiPSC-cortical neuron differentiation and maturation model and its*
588 *application to neurological disorders.* Stem Cell Reports, 2022. **17**(1): p. 96-109.
589 17. Vierbuchen, T., et al., *Direct conversion of fibroblasts to functional neurons by defined factors.*
590 Nature, 2010. **463**(7284): p. 1035-41.
591 18. Brennand, K.J., et al., *Modelling schizophrenia using human induced pluripotent stem cells.*
592 Nature, 2011. **473**(7346): p. 221-5.
593 19. Page, S.C., et al., *Electrophysiological measures from human iPSC-derived neurons are associated*
594 *with schizophrenia clinical status and predict individual cognitive performance.* Proc Natl Acad
595 Sci U S A, 2022. **119**(3).
596 20. Park, I.H., et al., *Disease-specific induced pluripotent stem cells.* Cell, 2008. **134**(5): p. 877-86.
597 21. Penney, J., W.T. Ralvenius, and L.H. Tsai, *Modeling Alzheimer's disease with iPSC-derived brain*
598 *cells.* Mol Psychiatry, 2020. **25**(1): p. 148-167.
599 22. Krieger, T.G., et al., *Modeling glioblastoma invasion using human brain organoids and single-cell*
600 *transcriptomics.* Neuro Oncol, 2020. **22**(8): p. 1138-1149.

601 23. Sancho-Martinez, I., et al., *Establishment of human iPSC-based models for the study and*
602 *targeting of glioma initiating cells.* Nat Commun, 2016. **7**: p. 10743.
603 24. Schloo, C. and L.M. Kutscher, *Modeling brain and neural crest neoplasms with human pluripotent*
604 *stem cells.* Neuro Oncol, 2023. **25**(7): p. 1225-1235.
605 25. Zhang, S., et al., *Development of human induced pluripotent stem cell (iPSC) line from a 60year*
606 *old female patient with multiple schwannoma.* Stem Cell Res, 2017. **19**: p. 31-33.
607 26. Langfelder, P. and S. Horvath, *WGCNA: an R package for weighted correlation network analysis.*
608 BMC Bioinformatics, 2008. **9**: p. 559.
609 27. Garcia-Moreno, A., et al., *Functional Enrichment Analysis of Regulatory Elements.* Biomedicines,
610 2022. **10**(3).
611 28. Wei, Z., et al., *A Subpopulation of Schwann Cell-Like Cells With Nerve Regeneration Signatures Is*
612 *Identified Through Single-Cell RNA Sequencing.* Front Physiol, 2021. **12**: p. 637924.
613 29. Gerber, D., et al., *Transcriptional profiling of mouse peripheral nerves to the single-cell level to*
614 *build a sciatic nerve ATlas (SNAT).* Elife, 2021. **10**.
615 30. Kim, H.S., et al., *Schwann Cell Precursors from Human Pluripotent Stem Cells as a Potential*
616 *Therapeutic Target for Myelin Repair.* Stem Cell Reports, 2017. **8**(6): p. 1714-1726.
617 31. Liu, Z., et al., *Specific marker expression and cell state of Schwann cells during culture in vitro.*
618 PLoS One, 2015. **10**(4): p. e0123278.
619 32. Chen, J., et al., *ToppGene Suite for gene list enrichment analysis and candidate gene*
620 *prioritization.* Nucleic Acids Res, 2009. **37**(Web Server issue): p. W305-11.
621 33. Hao, Y., et al., *Integrated analysis of multimodal single-cell data.* Cell, 2021. **184**(13): p. 3573-
622 3587 e29.
623 34. Choudhary, S. and R. Satija, *Comparison and evaluation of statistical error models for scRNA-seq.*
624 Genome Biol, 2022. **23**(1): p. 27.
625 35. Lause, J., P. Berens, and D. Kobak, *Analytic Pearson residuals for normalization of single-cell RNA-*
626 *seq UMI data.* Genome Biol, 2021. **22**(1): p. 258.
627 36. Korsunsky, I., et al., *Fast, sensitive and accurate integration of single-cell data with Harmony.* Nat
628 Methods, 2019. **16**(12): p. 1289-1296.
629 37. Tran, H.T.N., et al., *A benchmark of batch-effect correction methods for single-cell RNA*
630 *sequencing data.* Genome Biol, 2020. **21**(1): p. 12.
631 38. McInnes, L., J. Healy, and J. Melville, *Umap: Uniform manifold approximation and projection for*
632 *dimension reduction.* arXiv preprint arXiv:1802.03426, 2018.
633 39. Jiang, C., et al., *Basement membrane proteins in extracellular matrix characterize NF1*
634 *neurofibroma development and response to MEK inhibitor.* J Clin Invest, 2023. **133**(12).
635 40. Deng, B., *Mouse models and induced pluripotent stem cells in researching psychiatric disorders.*
636 Stem Cell Investig, 2017. **4**: p. 62.
637 41. Bashour, A.M., et al., *The neurofibromatosis type 2 gene product, merlin, reverses the F-actin*
638 *cytoskeletal defects in primary human Schwannoma cells.* Mol Cell Biol, 2002. **22**(4): p. 1150-7.
639 42. Hennigan, R.F., et al., *The NF2 tumor suppressor regulates microtubule-based vesicle trafficking*
640 *via a novel Rac, MLK and p38(SAPK) pathway.* Oncogene, 2013. **32**(9): p. 1135-43.
641 43. Shi, Q., et al., *Collagen Family Genes Associated with Risk of Recurrence after Radiation Therapy*
642 *for Vestibular Schwannoma and Pan-Cancer Analysis.* Dis Markers, 2021. **2021**: p. 7897994.
643 44. Kagan, H.M. and W. Li, *Lysyl oxidase: properties, specificity, and biological roles inside and*
644 *outside of the cell.* J Cell Biochem, 2003. **88**(4): p. 660-72.
645 45. Tu, Q., et al., *CDKN2B deletion is essential for pancreatic cancer development instead of*
646 *unmeaningful co-deletion due to juxtaposition to CDKN2A.* Oncogene, 2018. **37**(1): p. 128-138.
647 46. Wrensch, M., et al., *Variants in the CDKN2B and RTEL1 regions are associated with high-grade*
648 *glioma susceptibility.* Nat Genet, 2009. **41**(8): p. 905-8.

649 47. Xia, W., et al., *ANXA1 directs Schwann cells proliferation and migration to accelerate nerve*
650 *regeneration through the FPR2/AMPK pathway.* FASEB J, 2020. **34**(10): p. 13993-14005.

651